A Modeling Approach for Predicting the Abrasive Particle Motion During Chemical Mechanical Polishing

Elon J. Terrell

C. Fred Higgs III[1]
e-mail: higgs@andrew.cmu.edu

Department of Mechanical Engineering,
Carnegie Mellon University

Chemical mechanical polishing (CMP) is a manufacturing process in which a wafer surface is polished by pressing it against a rotating pad that is flooded with slurry. The slurry itself is a fluid containing abrasive particles. Past experimentation has shown that the distribution of suspended particles in the slurry is significantly related to the distribution of material removal on the wafer during CMP. Therefore, this study involves the development and simulation of a model that predicts the kinematics and trajectory of the abrasive particles. The simulation results compare well to data from shear cell experiments data conducted by other researchers. [DOI: 10.1115/1.2768614]

Keywords: chemical mechanical polishing, slurry particle motion, suspension flow

Introduction

Chemical mechanical polishing (CMP) has become a critical procedure for achieving surface planarization in small-scale devices and is commonly used as an intermediate fabrication step for such devices as integrated circuits (IC) and magnetic hard disk read/write heads. During the CMP process, the wafer that contains the devices is attached to a spinning disk that is pressed against a rotating polymeric pad that is flooded with chemically reactive slurry, as shown in Fig. 1. The slurry itself is a fluid that contains suspended abrasive nanoparticles. In a process we call particle augmented mixed-lubrication (PAML), the friction of the rotating pad and the abrasive particles causes the surface of the wafer to be polished (i.e., worn). Although CMP is commonly practiced in industry as a part of IC fabrication, much of the phenomena behind CMP are not understood due to complex slurry fluid motion and the interactions between the wafer, pad, and the abrasive particles. These complexities are oftentimes the cause of unpredictable and nonuniform material removal on the thin-film surface. Thus, CMP research is necessary in order to gain insight into the science behind the process as well as to develop a reliable model that allows the surface wear (or material removal) distribution to be accurately predicted.

A number of past studies have been conducted in order to create models for the prediction of CMP. Several studies have used contact mechanics modeling, assuming that the majority of wafer surface wear takes place due to the friction between the wafer and pad surfaces [1–3]. Other studies have focused on the flow field of the slurry at the wafer/pad interface, assuming that the wafer and pad surfaces are completely separated by the slurry film during CMP [4–7]. Further studies have been conducted that use a combination of contact mechanics and slurry hydrodynamic analysis methods [8,9]. However, it has been found that the abrasive particle distribution has an effect on the material removal rate (MRR) of wafer films, which gives rise to the need for further understanding of the motion and MRR of the abrasive particles during CMP [10]. As a preliminary step, the focus of this study is the modeling and simulation of abrasive nanoparticle motion during CMP.

Several studies have been conducted to analyze the motion of suspended particles in a fluid medium, although very few of them have been related to CMP. Both Lin et al. [11] and Shen and Bogy [12] studied the motion of contamination particles in the air gap of a hard disk drive slider bearing. Both of their studies used continuum modeling to predict the airflow field. The applied forces from the flow field were then used to calculate the trajectories of the particles over time. However, both of their studies analyzed particle flow in an air slider bearing domain, which is different from a CMP-type domain. Zettner and Yoda [13] used a fluorescent imaging technique to analyze the average velocity and shear rate of particles in a simplified CMP-type flow domain. However, their empirical study provided no insight into the discrete, localized motion of the particles.

The focus of this study was to model and simulate the motion of suspended abrasive nanoparticles in slurry during CMP. This study used a combination of continuum modeling and particle dynamics to track the motion of abrasive particles in a CMP-type domain. The model tracked the motion of many particles in the wafer-pad interface and thus serves as an expansion of a previous study by Terrell et al. [14], which tracked the motion of a single particle during CMP. It is important to note that this model assumed that the wafer and pad surfaces were completely separated by slurry (i.e., hydrodynamic lubrication), thus neglecting the effect of solid-solid contact between the two surfaces. Although a number of studies have shown that contact-based wear is of primary importance in CMP [1–3,15], this contact phenomenon is neglected in this study in order to focus on analyzing the motion of the abrasive particles.

Similar to the studies of Lin et al. [11] and Shen and Bogy [12], a continuum approach was used in this study to analyze the flow field of the particle-free slurry. The motion of the particles, meanwhile, was determined by modeling the applied forces on each particle and modeling particle-particle and particle-wall collisions.

The model created in this study is first compared to the generalized experimental shear cell test results of Ng et al. [16] and Shapley et al. [17] before being simulated for a simplified CMP geometry. The CMP simulation results are then presented in terms of the particle velocity profile and the frequency of particle collisions with the wafer surface. The effects of two input parameters

[1]Corresponding author.

Contributed by the Tribology Division of ASME for publication in the JOURNAL OF TRIBOLOGY. Manuscript received March 17, 2006; final manuscript received April 18, 2007. Review conducted by Hong Liang. Paper presented at the STLE/ASME 2006 International Joint Tribology Conference (TRIB2006), October 22–25, 2006, San Antonio, TX.

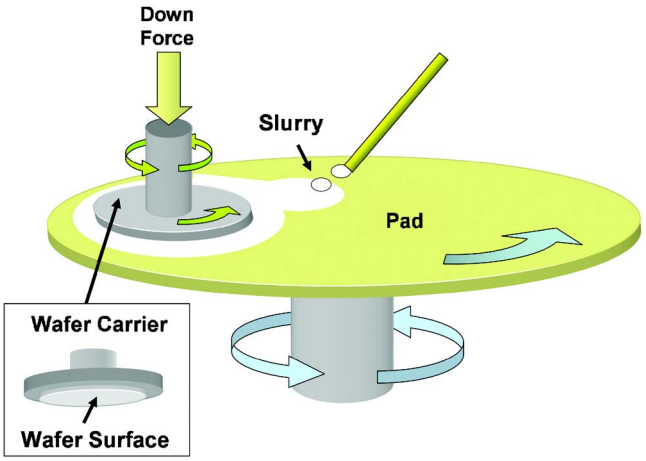

Fig. 1 Diagram of the CMP process

are analyzed in this study: (i) the location of the focus area within the wafer-pad interface and (ii) the adjusted vertical location of the wafer surface.

Overview of Slurry Flow Model

In this study, the CMP process was modeled by simplifying the domain into a two-dimensional area that consists of the slurry between the wafer/pad gap along a one-dimensional line, as shown in Fig. 2(*a*). In most CMP processes, the wafer surface is relatively smooth compared to the rough pad surface. Therefore, the wafer surface was assumed to be flat and stationary, while the typically random rough pad surface was idealized as a traveling sine wave according to the following:

$$h_f(x,t) = h_m(x) + R_P \sin\left[\frac{2\pi}{\lambda}(x - Ut)\right] \tag{1}$$

where R_p is the peak surface roughness, U is the velocity of the bottom surface, λ is the peak-to-peak length of each asperity, t is the time of the simulation, and x is the horizontal distance along the wafer. The parameter $h_m(x)$ is the mean asperity location of the pad. It was assumed that the pad deflects continuously under the wafer; thus, the mean asperity location was a function of x only. The resulting simulation domain is shown in Fig. 2(*b*).

The model in this study first solves for the flow field of particle-free slurry, then seeds particles in the domain and tracks their motion using a Euler-type time-stepping algorithm. The placement of the particles in the domain was done randomly, while the number of particles in the domain was calculated from the user-defined solid fraction v_s, as follows:

$$v_s = \frac{N_p V_p}{V_d} \tag{2}$$

where V_d is the volume of the domain of interest, V_p is the volume of the largest particle in the domain, and N_p is the number of particles in the domain.

Continuum Modeling

The two-dimensional flow field of the particle-free slurry was first modeled using a continuum approach before being seeded with abrasive particles. Water was assumed to be the carrier fluid for the abrasive particles because of the similar fluid properties between water and particle-free slurry. It was also assumed that the wafer/pad gap thickness was small compared to the length of the wafer, which allowed the fluid to be assumed as laminar. The slurry flow field was subject to the following boundary conditions for the x-velocity component, $u(x,y,t)$, and the y-velocity component, $v(x,y,t)$:

$$u(x,y_{\text{wafer}},t) = v(x,y_{\text{wafer}},t) = 0 \tag{3a}$$

$$u(x,h_f,t) = v(x,h_f,t) = U \tag{3b}$$

Assuming that the wafer surface is located at $y=0$ and moving at speed U, the horizontal velocity profile of the particle-free slurry was calculated as a Couette/Poiseuille flow

$$u(x,y,t) = \frac{1}{2\mu}\frac{dp}{dx}y[y - h_f(x,t)] + U\frac{y}{h_f(x,t)} \tag{4}$$

where μ is the dynamic viscosity of the particle-free fluid. The hydrodynamic pressure distribution $p=p(x)$ from Eq. (3) was determined using the one-dimensional Reynolds equation, given as follows:

$$\frac{d}{dx}\left(h_m(x)^3\frac{dp}{dx}\right) = 6\mu U\frac{dh_m(x)}{dx} \tag{5}$$

After the horizontal velocity profile of the particle-free slurry was fully defined, the vertical velocity profile was then calculated by applying the continuity equation to the horizontal velocity profile. The vertical velocity profile was thus calculated to be the following:

$$v(x,y,t) = \frac{y^2}{\mu}\left(\frac{y}{6}\frac{d^2p}{dx^2} + \frac{h_f}{4}\frac{d^2p}{dx^2} + \frac{1}{4}\frac{\partial h_f}{\partial x}\frac{dp}{dx}\right) + \frac{Uy^2}{2h_f^2}\frac{\partial h_f}{\partial x} \tag{6}$$

where $h_f=h_f(x,t)$.

The resultant velocity field of the particle-free slurry at an instant in time was simulated and is shown by the velocity vectors in Fig. 3. The movement of the bottom surface caused periodic changes in the velocity field of the particle-free slurry with time.

Particle Dynamics Modeling

A common source of complication for solid/liquid two-phase flow problems is determining how the different phases affect each

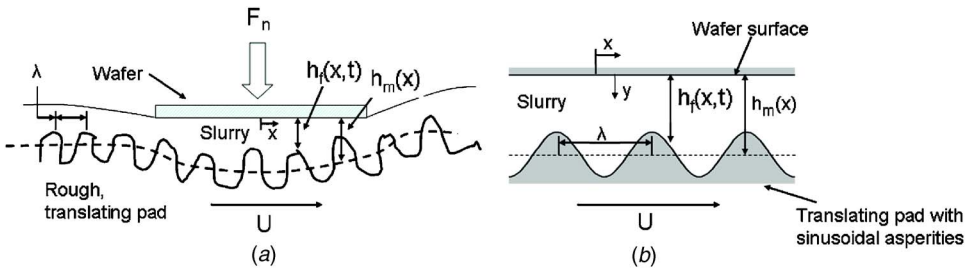

Fig. 2 One-dimensional diagram of a CMP process, and the simplified modeling domain defined in the current study

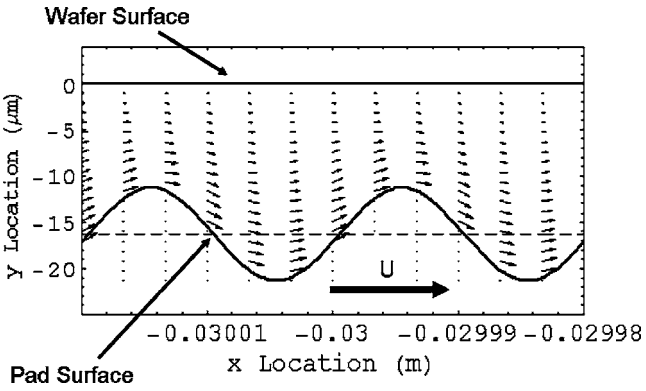

Fig. 3 Simulation output of velocity vectors of particle-free slurry flow field

other in the domain. Complex iteration schemes are often necessary for calculating the relative effects of each phase. In this study, however, it was assumed that the presence of the particles would have a negligible effect on the flow field of the particle-free fluid in CMP slurry. This argument was first based on the fact that the size of an individual particle is relatively small compared to the volume of the wafer/pad interface. Additionally, this study assumed that the slurry contained a dilute concentration of particles, which is typical of many CMP slurries [18,19]. Therefore, the model in this study could then calculate the fluid motion independent of the particle motion.

The motion of a particle in the slurry was modeled after the flow field of the particle-free slurry was fully defined. The particle motion was modeled by accounting for the forces acting on it. The governing equations for the particle motion are given as follows:

$$\frac{dx_p}{dt} = u_p \tag{7a}$$

$$\frac{dy_p}{dt} = v_p \tag{7b}$$

$$m_p \frac{du_p}{dt} = f_{\text{drag},x} + f_{\text{saff},x} + f_{\text{hydro}} \tag{8a}$$

$$m_p \frac{dv_p}{dt} = f_{\text{drag},y} + f_{\text{saff},y} + f_{gb} \tag{8b}$$

where x_p, y_p, u_p, and v_p are the horizontal location and vertical location, horizontal velocity, and vertical velocity of the particle, respectively. Equations (8*a*) and (8*b*) also include $f_{\text{drag},x}$ and $f_{\text{drag},y}$, the horizontal and vertical drag force, respectively; $f_{\text{saff},x}$ and $f_{\text{saff},y}$, the horizontal and vertical Saffman forces, respectively; f_{hydro}, the force due to the hydrodynamic pressure gradient; and $f_{g/b}$, the gravity and buoyancy forces. A description of each of the forces is contained in the following paragraph.

Drag Force. Assuming the abrasive particles were spherical, the drag force for creeping flow over each particle was given as follows:

$$f_{\text{drag},x} = 6\pi\mu a_p[u(x_p,y_p,t) - u_p] \tag{9a}$$

$$f_{\text{drag},x} = 6\pi\mu a_p[v(x_p,y_p,t) - v_p] \tag{9b}$$

where a_p is the radius of the particle. Because the velocity field of the particle-free slurry is nonuniform and periodically transient, the drag force on the particle varies, depending on its location and the time of the simulation.

Hydrodynamic Force. The particle will also experience a net force from the hydrodynamic pressure gradient of the particle-free slurry. A simplified expression for the hydrodynamic pressure gradient can be found by assuming that a uniform pressure difference is applied across the streamwise width of the particle.

The hydrodynamic force can thus be estimated as follows:

$$f_{\text{hydro}} = -\pi a_p^2\left(2a_p\frac{dp}{dx}\right) = -2\pi a_p^3\frac{dp}{dx} \tag{10}$$

By applying lubrication theory to the CMP problem, it is found that the hydrodynamic pressure gradient is only expected to vary in the horizontal direction. Therefore, the hydrodynamic force acts only in the horizontal direction and is only a function of the downstream coordinate x.

Gravity/Buoyancy Force. The abrasive particles all experience a constant body force due to gravity and buoyancy from the surrounding fluid, given as follows:

$$f_{gb} = \frac{4}{3}\pi a_p^3(\rho - \rho_p)g \tag{11}$$

where ρ and ρ_p are the densities of the fluid and of the particle, respectively, and g is the acceleration due to gravity. This force is constant and acts only in the vertical direction.

Saffman Force. Saffman [20] predicted that submicron particles in shear flow experience a force that acts perpendicular to the direction of shear. Past studies have used this force in predicting particle dynamics in air slider bearings [11,12]. The Saffman lift force is given as follows:

$$f_{\text{saff},x} = 6.46a_p^2(\rho\mu)^{0.5}\left|\frac{dv}{dx}\right|^{0.5}[v(x_p,y_p,t) - v_p] \tag{12a}$$

$$f_{\text{saff},y} = 6.46a_p^2(\rho\mu)^{0.5}\left|\frac{du}{dx}\right|^{0.5}[u(x_p,y_p,t) - u_p] \tag{12b}$$

The Saffman force varies with respect to the location of the particle and the simulation time.

Magnus Force. The abrasive particles in this model were assumed to freely rotate due to the moments imposed by the shearing fluid and the pad and wafer boundaries. Suspension theory dictates that rotating particles in a flow field experience a perpendicular force, known as Magnus force, due to an inertial "shear-spin" effect from the surrounding fluid [21]. However, in his study, Saffman determined by dimensional analysis that the Magnus force would be less than an order of magnitude smaller than the Saffman force for freely rotating particles in low-Reynolds number shear flow [20]. Thus, the Magnus force was neglected in this study. The neglect of Magnus force in comparison to Saffman force has precedence in past particle flow models, such as in the air bearing particle contamination studies by Bogy and collaborators [12,22].

Inertial and Brownian Effects. In order to develop a model that accounts for all the applied forces on each abrasive particle, it is important to investigate the effects of particle inertia and Brownian motion. These effects can be defined from two nondimensional parameters that are extracted from suspension theory.

The parameter that describes the effect of particle inertia is the particle Reynolds number, which determines the relative effect of particle inertia to the viscosity of the suspending fluid [23]. The particle Reynolds number is defined as follows:

$$\text{Re}_p = \frac{\rho\dot{\gamma}_m a_p^2}{\mu} \tag{13}$$

where $\dot{\gamma}_m = U/h_m$ is the mean shear rate, which ranges between 23,900 s^{-1} and 34,400 s^{-1} for the CMP geometry in this study. Using the shear rate parameter and the other parameters whose values for a typical CMP process are defined in Table 2, the particle Reynolds number can be found to be approximately Re_p

$=5.8\times10^{-4}$. Since $\mathrm{Re}_p \ll 0.1$, then particle inertial effects can be ignored according to suspension theory [17,23].

The nondimensional parameter that describes the effect of Brownian motion is the Brownian Peclet number, which provides a relative weighting between the hydrodynamic force and the Brownian force applied to a particle in a suspending medium [23]. The Brownian Peclet number is defined as follows:

$$\mathrm{Pe} = \frac{\dot{\gamma}}{D_r} \tag{14}$$

where D_r is the rotary Brownian diffusion coefficient, which for hard spheres is defined as the following:

$$D_r = \frac{kT}{8\pi\mu a_p^3} \tag{15}$$

where k is the Stefan–Boltzmann constant and T is the absolute temperature. Assuming an ambient temperature of 300 K and typical CMP parameters as defined in Table 2, the Brownian Peclet number was found to be approximately $\mathrm{Pe}=700$. Since the Brownian Peclet number is significantly greater than unity, it was assumed that the effect of Brownian forces can be neglected.

Electrostatic Forces. Electrostatic effects in CMP have been found to depend greatly on a number of parameters, such as the slurry pH, the material composition of the slurry abrasives, and the material that is being polished. At their most obvious level, the electrostatic forces are seen to affect the agglomeration of abrasive particles [24]. This phenomenon can be easily captured in this model by varying the size distribution of the abrasive particles. However, accounting for the electrostatic interactions between the particles and the wafer and the particle and the pad requires specific details about the type of polishing that is being modeled [25]. Therefore, only mechanical interactions were analyzed in this model in order to preserve its generic aspect, and for simplification purposes.

Modeling of Particle Collision Behavior

In the present study, the electrostatic forces between particles are assumed negligible. However, the particles in the domain were allowed to undergo particle-particle collisions and surface-particle collisions. All collisions were modeled using particle dynamic formulations, assuming that a single particle collided with only one other body at a given time.

According to collision theory, the post-collision velocity of two colliding objects can be found by solving the conservation of momentum and coefficient of restitution equations, given as follows:

$$m_1 v_1 + m_2 v_2 = m_1 v_1' + m_2 v_2' \tag{16a}$$

$$\varepsilon = \frac{v_2' - v_1'}{v_1 - v_2} \tag{16b}$$

where v_1 and v_1' are the pre- and post-collision velocities of the first colliding particle, respectively, along the line of collision, while v_2, and v_2' are the pre- and post-collision velocities of the second colliding particle along the line of collision. The parameter ε is the coefficient of restitution between the two colliding objects. A coefficient of restitution of $\varepsilon=1$ indicates a perfectly elastic collision, whereas $\varepsilon=0$ indicates a perfectly inelastic collision. The velocities of each object normal to the direction of collision can be assumed to be unchanged during the collision.

Although the coefficient of restitution for many colliding objects is near unity when both objects are dry (immersed in air), a number of past studies have shown that the coefficient of restitution tends to decrease significantly when the colliding objects are "wet" (immersed in a fluid). Past studies [26–28] have modeled and measured the parameter $\varepsilon_{\mathrm{wet}}/\varepsilon_{\mathrm{dry}}$ for a number of different fluids, in which the parameter $\varepsilon_{\mathrm{wet}}/\varepsilon_{\mathrm{dry}}$ is the ratio between the wet and the dry coefficient of restitutions between two colliding objects. They found that $\varepsilon_{\mathrm{wet}}/\varepsilon_{\mathrm{dry}}$ was highly dependent on the nondimensional impact Stokes number, which is defined as follows:

$$\mathrm{St} = \frac{(2/9)\rho_p(v_1 - v_2)a_p}{\mu} \tag{17}$$

Each of the immersed collision studies found that $\varepsilon_{\mathrm{wet}}/\varepsilon_{\mathrm{dry}}$ was approximately zero when the Stokes number was less than some critical value, and then gradually increased to unity as the Stokes number increased logarithmically. From Joseph et al.'s [28] and Gondret et al.'s [27] studies, the critical Stokes number was $\mathrm{St}_{cr} \approx 10$, while from Davis' and Serayssol's [26] lubrication model $\mathrm{St}_{cr} \approx 5$. Thus, when two colliding objects are immersed in a fluid that is dominated by viscous effects, their collision will be mostly inelastic.

In the current study, it was important to know the relative elasticity or inelasticity of the collisions between two particles or between a particle and one of the surfaces of the domain. Therefore, a typical impact Stokes number for this study was calculated using the CMP parameters as defined in Table 1, assuming that the bottom wall velocity U can be substituted for the impact velocity $(v_1 - v_2)$ because they are of the same order of magnitude. The impact Stokes number for this CMP study was thus calculated to be $\mathrm{St} \approx 0.1$, which is less than the critical Stokes number of $\mathrm{St}_{cr} = 5$ from Davis' and Serayssol's [26] study. Therefore, the coefficient of restitution between all objects in this study could be assumed to be zero, which implies completely inelastic collisions.

Table 1 Parameters used in particle flow simulation in order to compare to the experimental tests of Shapley et al. [17]

Parameter	Value
Fluid	$\rho=1183$ kg/m^3
	$\mu=0.84$ Pa s
Particles	$\rho_p=1183$ kg/m^3
	90 μm $< a_p <$ 106 μm
Bounding surfaces	No roughness
	$U=5.98$ cm/s

Simulation Procedure

The particle tracking simulations were run using a time-stepping algorithm in the MATHEMATICA® programing environment. The simulation first solves for the velocity field of the particle-free slurry as a function of the area of focus on the wafer and the vertical location of the wafer surface. The simulation then placed particles in random locations in the area of focus, where the number of particles is determined from the user-defined solid fraction.

After the initial locations of the particles were defined, the simulation stepped through time to model particle collisions or movements due to the applied forces from Eq. (8). For each time step, the simulation first checked each particle to determine whether it was colliding with another particle, the wafer, or the pad surface. If a collision event was found for a given particle, the velocity of the particle would be adjusted as described in the previous section. If the given particle was not in a collision event, then its acceleration due to applied forces would be calculated. The horizontal and vertical velocity components of each particle would then be updated according to the following:

$$u_p|_{t+\Delta t} = u_p|_t + \frac{du_p}{dt}\Delta t \tag{18a}$$

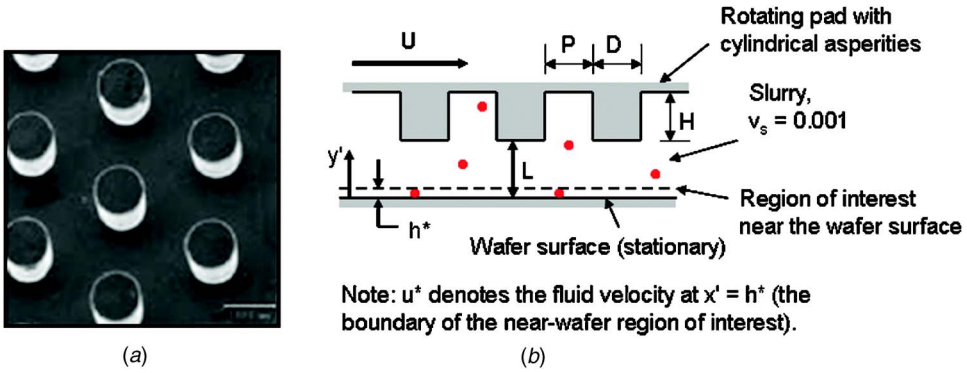

Fig. 4 (*a*) **SEM image of the simulated "pad" surface used in the particle flow visualization experiments by Ng et al. [16] and (*b*) two-dimensional diagram of the simplified CMP domain of Ng et al. [16]**

$$v_p|_{t+\Delta t} = v_p|_t + \frac{dv_p}{dt}\Delta t \tag{18b}$$

where du_p/dt and dv_p/dt are the horizontal and vertical components of acceleration as given in Eqs. (8*a*) and (8*b*).

After the velocity components of each particle were recalculated from collision or applied force modeling, the positions of each particle were updated according to the following:

$$x_p|_{t+\Delta t} = x_p|_t + u_p\Delta t \tag{19a}$$

$$y_p|_{t+\Delta t} = y_p|_t + v_p\Delta t \tag{19b}$$

The simulated domain was modeled with periodic boundary conditions, such that any particle that traveled downstream of the domain was replaced at the same vertical location immediately upstream of the domain. The particle tracking took place over a simulated time period of $t_{sim}=0.0025$ s. The nanometer-scale radii of the abrasive particles necessitated the use of time steps on the order of $\Delta t \approx 10^{-8}$ s or smaller to correctly resolve the acceleration changes in Eqs. (8*a*) and (8*b*).

Comparisons to Experimental Data

The model was compared with two different experimental studies [16,17] in order to determine how well it could predict the velocity profile of an actual particle suspension shear flow. This was done for the purpose of validating the current model against the appropriate experiments that were found in the literature.

Comparison 1: Ng et al. [16] Experiments Versus Model. The model was first compared to a CMP-type shear cell experiment by Ng et al. [16], who used an evanescent wave technique to visualize the motion of fluid with suspended nanoparticles between a fixed, smooth, nonrotating disk (simulating the wafer) and a rough, rotating disk (simulating the pad, as shown in Fig. 4(*a*)). As Fig. 4(*b*) shows, the simulated wafer and pad were held a fixed distance apart. Visualization experiments were conducted at various pad speeds (denoted as U) and wafer-pad distances (denoted as L), which were combined into a single input parameter called the shear cell Reynolds number, given as follows:

$$\mathrm{Re}_{\mathrm{shear}} = \frac{UL}{\mu} \tag{20}$$

where μ is the viscosity of the particle-free fluid. The evanescent wave method allowed the particles that were closest to the wafer surface to be visualized, and thus, the overall velocity of near-wafer particles was measured with respect to various values of the shear cell Reynolds number.

The model developed in the current study was adapted to simulate the experimental setup of Ng et al.'s [16] study as closely as possible. The sinusoidal pad surface of the model was specified to have a topography of similar roughness as the rough "pad" in Ng et al.'s [16] study. Additionally, the wafer surface was held a fixed distance away from the pad surface, resulting in a simulation domain as shown in Fig. 5. The hydrodynamic pressure field of the model was specified to be zero inside the gap. The particle flow simulations were conducted using film thickness inputs of $L=25$ μm, 50 μm, and 100 μm, while the pad speed U was varied in order to match the shear cell Reynolds numbers of Re=0.2, 0.4, 0.6, and 0.8. To be consistent with experiment, only the particles within $y'=h^*=250$ nm of the wafer surface were analyzed from the simulation results. The ensemble average velocity of the near-wall particles were calculated for each simulation in order to compare to Ng et al.'s [16] data. The near-wall velocities of the particles are normalized by u^*, which is the velocity of the flow field at the near-wall distance of $y'=h^*$.

The simulation results, compared to Ng et al.'s [16] experimental measurements, are shown in Fig. 6 for three different film thickness variations. The model predicts that the particles would be accelerated to almost the same speed as the surrounding flow field ($u/u^*=1$). This prediction agrees well with Ng et al.'s [16] experimental results for a film thickness of $L=100$ μm, although there is significant disagreement with the results at film thicknesses of $L=25$ μm and $L=50$ μm. The reason for this difference can possibly be attributed to the increased uncertainty of the film thickness in Ng et al.'s [16] test rig because the gap height was decreased, as stated in their paper.

Comparison 2: Shapley et al. [17] Experiments Versus Model. The model was also compared to the experimental data of Shapley et al. [17], who measured the velocity profile of a particle suspension inside a narrow-gap Couette shear cell using laser Doppler velocimetry (LDV). The shear cell consisted of two concentric cylinders, with the inner cylinder rotating at an angular velocity of $\Omega=10$ rpm and the outer cylinder fixed (Figs. 7(*a*) and 7(*b*)). Although the majority of Shapley et al.'s [17] measurements

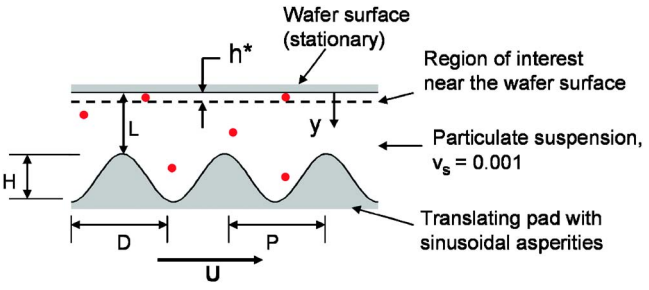

Fig. 5 Diagram of the modeling domain from the current study that emulated the shear cell experiment by Ng et al. [16]

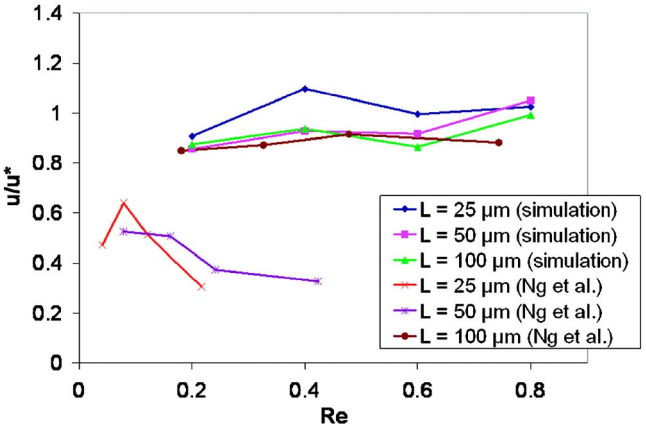

Fig. 6 Comparison between the near-wall particle velocity measured by Ng et al. [16] and the corresponding velocity extracted from the simulation of the current study

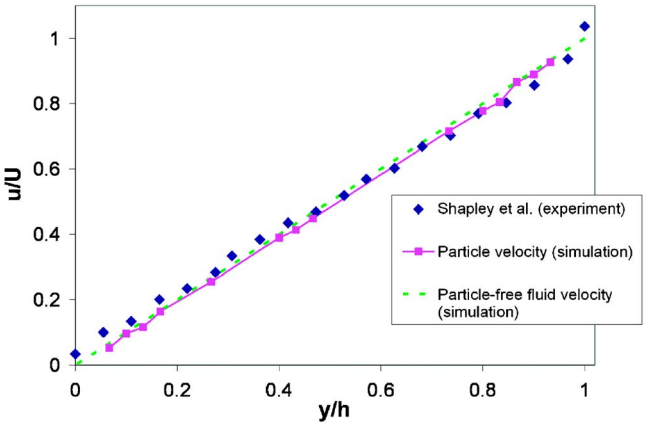

Fig. 8 Comparison between Shapley et al.'s [17] experimental data and the results from simulation

pertained to particle velocity fluctuations, they also conducted a set of steady-state velocity profile measurements at a dilute solid fraction for baseline measurement purposes. In order to compare to Shapley et al.'s [17] experimental results, the particle flow model was input with similar test parameters, as outlined in Table 1. The model was adapted to have completely flat top and bottom surfaces, as opposed to the sinusoidal bottom surface which simulated the roughness of the polishing pad in CMP.

The particle velocity profile from the simulation is compared to Shapley et al.'s [17] experimental velocity profile in Fig. 8. From linear interpolation of the data, the model is found to predict the measured particle velocity profile from Shapley et al. [17] to within a maximum percent error of 9%.

CMP Geometry Simulation

In order to model an actual CMP geometry, this study expanded upon the formulation of Shan et al.'s CMP model [29], which predicted a hydrodynamic pressure field with a subambient region. Table 2 shows the additional parameters that were used for the simulation. Similar to commercial CMP slurry, the solid fraction in this study was maintained at a constant $\nu_s=0.0029$.

The wafer-pad interface geometry was based on the results of Shan et al. [29], who used a contact stress model to determine the film thickness distribution at the wafer/pad interface during CMP along a one-dimensional constant pad velocity line. The film thickness distribution from Shan et al.'s [29] study, which was smallest at the edges of the wafer and largest in the middle, was used in the current study as the expression for the vertical location of the pad mean line, $h_m(x)$. In order to conserve computational time, each of the simulations analyzed a small "focus area" at various wafer-pad interface locations along the constant pad velocity line. Diagrams of the constant pad velocity lines and the focus areas are shown in Figs. 9(*a*) and 9(*b*).

The coordinate system of the simulated CMP domain is given by Fig. 10. The location of $x=0$ corresponded to the center of the wafer domain, while the left and right edges of the wafer are located at $x=-0.045$ m and $x=0.045$ m, respectively. Simulations were performed at different focus areas, as discussed previously and depicted in Figs. 12 and 14. Each of the focus areas was centered at a downstream (x) location denoted as x_{focus}, and each of the areas had a downstream (x) length of $L_{\text{focus}}=100$ μm. The focus areas that were tested were located at $x_{\text{focus}}=-0.03$ m, -0.01 m, 0.01 m, and 0.03 m. It is important to note that the mean film thickness $h_m(x)$ changed, depending on the location of the focus area according to the film thickness distribution from Shan et al. [29].

In the vertical direction, $y=0$ corresponded to the unadjusted location of the wafer surface, while $y=h(x,t)$ corresponded to the location of the pad asperity at a given horizontal location and time. The adjusted location of the wafer surface was varied between $y_{\text{wafer}}=0$ μm and $y_{\text{wafer}}=8$ μm in order to determine the effect of a thinner wafer/pad interface on the particle motion.

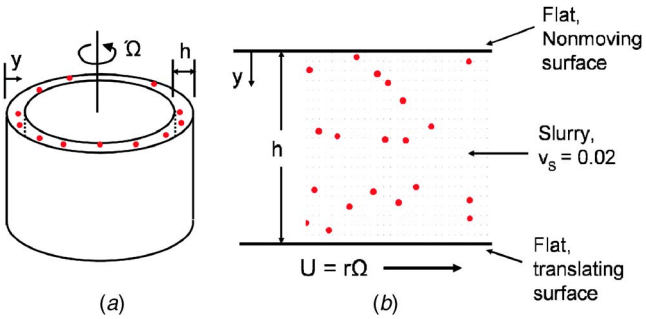

Fig. 7 (*a*) Diagram of the Couette shear cell domain of Shapley et al. [17] and (*b*) the simulation domain that was defined in order to compare to Shapley et al.'s experimental results

Results and Discussion

A series of numerical simulations were conducted in order to analyze the effects of wafer position on the motion of the particles at different locations across the wafer/pad interface. Simulating the experimental setup of Shan et al. [29], the wafer is stationary while the pad rotates, as shown in Fig. 2. For each of the simulations, the nanoparticles were placed in random locations the interface domain with zero initial velocity. A sample image of the initial locations of the particles is shown in Fig. 11. After the simulation was started, it was found that the particles that were initially placed in the middle of the wafer/pad gap were almost immediately accelerated to the velocity of the surrounding flow

Table 2 Parameters used in particle tracking simulation

Parameter	Value
Fluid	$\rho=1183$ kg/m^3
	$\mu=0.84$ Pa s
Particles	$\rho_p=3970$ kg/m^3
	150 nm $< a_p <$ 200 nm
Pad	$R_p=5$ μm
	$\lambda=20$ μm
	$U=0.43$ m/s

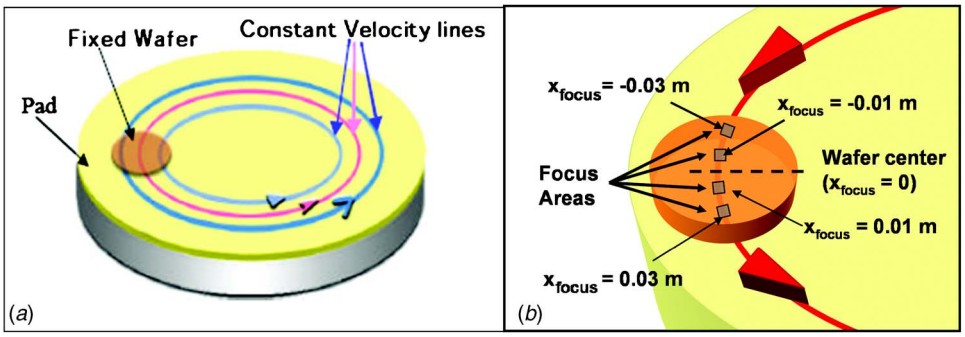

Fig. 9 Diagrams showing (*a*) the constant pad velocity lines during CMP and (*b*) the discrete focus areas in the wafer-pad interface

field. The particles in the middle of the gap traveled primarily in the horizontal direction but had an oscillatory vertical motion as they were passed by the traveling asperities. It was also observed that any particle that came near an asperity valley was drawn into the bottom of the valley and remained there for the duration of the simulation.

The average velocity of the particles in the domain was calculated by averaging the velocity of each particle over all of the time steps in each simulation. It was assumed that any start-up effects would be negligible due to the fact that the particles were quickly accelerated by the flow field after the simulation started. The average particle velocity as a function of the wafer's separation distance from the pad surface is shown in Fig. 12, where it appears that the particle velocity is generally highest at $x_{focus}=-0.03$ m and lowest at $x_{focus}=0.01$ m. This occurrence is most likely attributed to the acceleration and deceleration of the flow field caused by the changing film thickness, as the mean film thickness was relatively small at $x_{focus}=-0.03$ m and relatively large at $x_{focus}=0.01$ m.

The time-averaged particle velocity profiles were calculated by dividing the vertical distance of the flow domain into equally sized bins and determining the average particle velocity for each bin for all time steps.

The velocity profiles are first shown with an "unadjusted" (recall Fig. 10) wafer surface height ($y_{wafer}=0$) for each focus area along the constant pad velocity line. These particle velocities, compared to the time-averaged velocity profile of the surrounding fluid, are shown in Figs. 13(*a*)–13(*d*). Figures 13(*a*)–13(*d*) show that the particle velocity profiles follow the same globally decreasing trend as the fluid velocity profiles, but appear to be moving slightly faster than the local fluid directly above the asperities. It is possible that this increase in particle velocity was caused by the periodic acceleration of fluid from beneath the particle, which occurred when the particle was being passed by an asperity.

An average velocity profile of the nanoparticles was calculated as a function of the adjusted wafer surface height (y_{wafer}) for each focus area. The average particle velocity profiles for different values of y_{wafer} at the focus area of $x_{focus}=0.01$ m is shown in Fig. 14. As Fig. 14 shows, the particle velocity profiles had similar trends around the region where the asperities were located, with the average particle velocity about the same as the velocity of the pad. The velocities of the particles in this region showed a significant amount of scatter that was most likely due to the effect of the rapidly changing flow field on the particle. In the region above the asperities, it appeared that the particle velocity profile showed an increasingly sharper gradient near the wafer surface as the vertical wafer surface position was lowered. This implies that an increased amount of particle shearing would occur when the wafer surface position is lowered toward the pad.

The number of particle collisions with the wafer surface was also recorded for each simulation. It was expected that the number

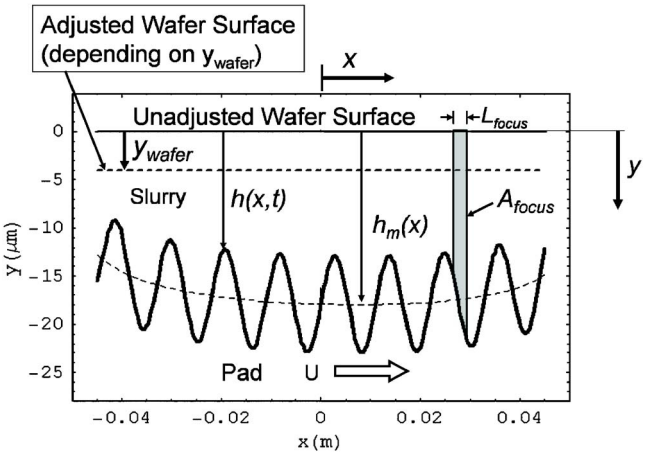

Fig. 10 Diagram delineating the simulation domain

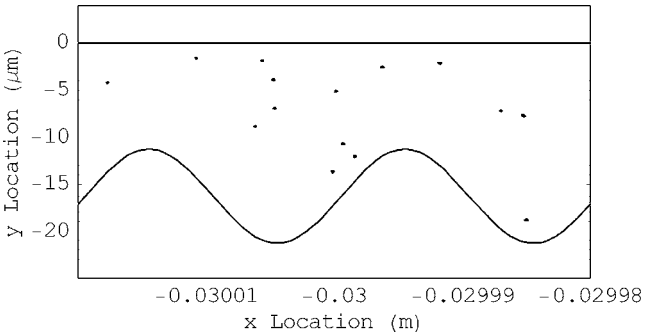

Fig. 11 Wafer-pad interface domain showing locations of abrasive particles

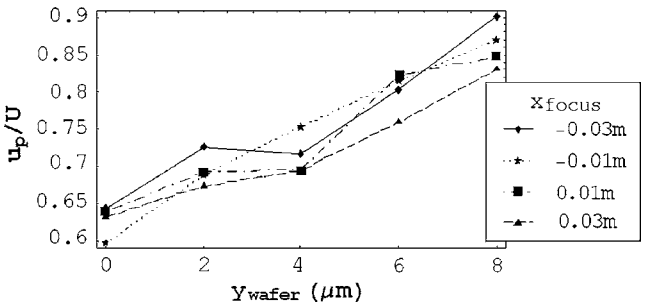

Fig. 12 Effect of wafer height on the ensemble average particle velocity

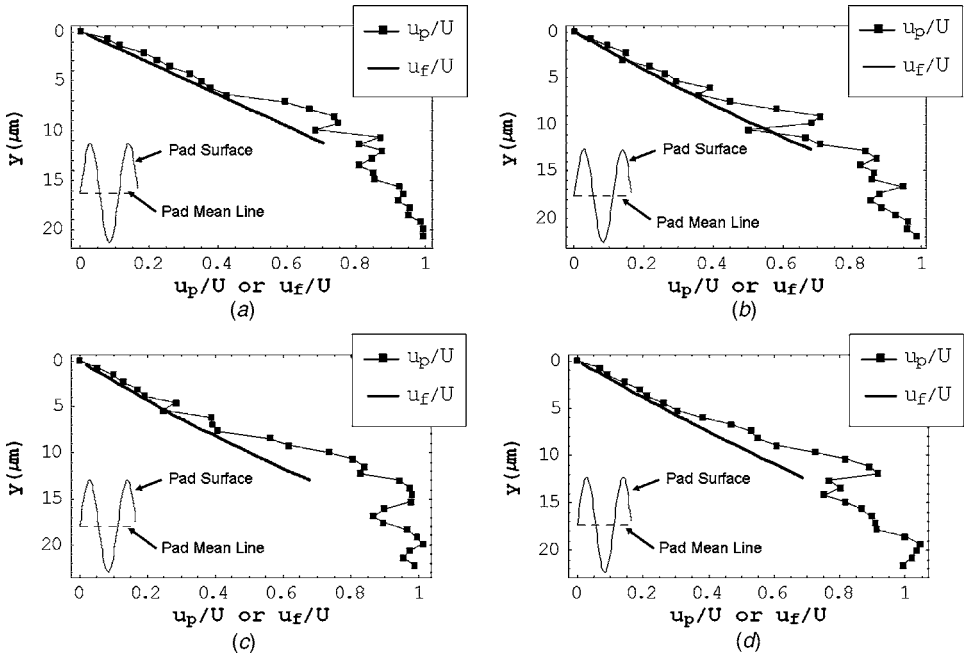

Fig. 13 Time-averaged particle velocity profile at (*a*) $x_{focus}=-0.03$ m, (*b*) $x_{focus}=-0.01$ m, (*c*) $x_{focus}=0.01$ m, and (*d*) $x_{focus}=-0.01$ m, compared to the fluid velocity

of collisions is related to the amount of abrasive wear that takes place during CMP. The number of wafer surface collisions is shown in Fig. 15, where the number of top wall collisions generally increases as the wafer surface position is lowered toward the pad. However, it appears the collision frequency in the focus area of $x_{focus}=-0.03$ m is affected by wafer position much more strongly than in the other locations. The mean film thickness, from Shan et al. [29], is the smallest in this region, which possibly means that the wafer surface collisions were drastically increased because the particles had less room to travel in the vertical direction.

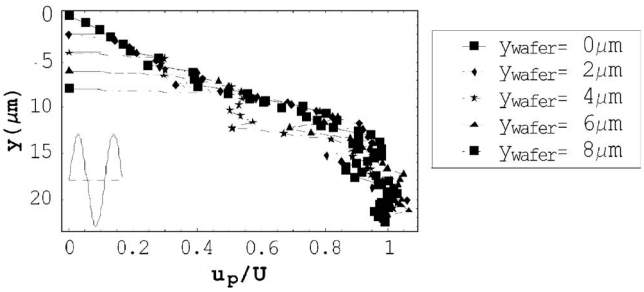

Fig. 14 Time-averaged particle velocity profile as a function of y_{wafer}, $x_{focus}=0.01$ m

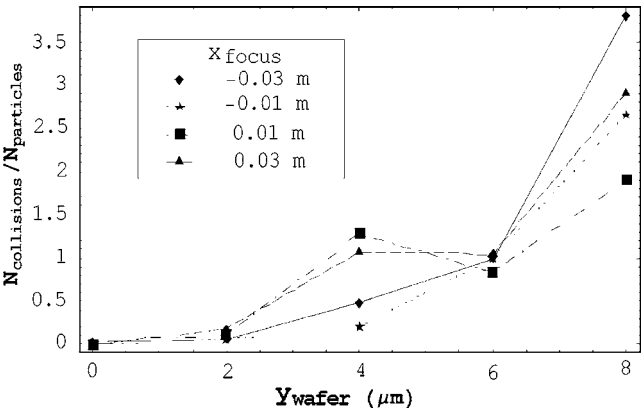

Fig. 15 Number of particle collisions with the wafer surface for each simulation

Conclusion

The motion of nanoparticles in slurry was analyzed using a hybrid approach of continuum analysis, particle kinetic modeling, and particle dynamic modeling. It was found that particles in the gap between the asperities and the wafer surface tended to travel slightly faster than the local fluid velocity, and the particles that traveled into an asperity valley were drawn into the bottom of the valley. Additionally, it was found that lowering the wafer toward the pad caused the particle velocity profile to show an increased amount of shear and also causes an increase in the frequency of particle collisions with the wafer surface.

These results suggest that the potential for abrasive wear of the wafer surface drastically increases as the wafer is lowered toward the pad, even if the wafer is not in contact with the pad. Studies have indicated that the main sources of wafer surface wear are abrasive particles that become trapped between the wafer and the pad. It will thus be interesting to further expand this simulation to determine how a further decrease in wafer height will affect the velocity distribution and wafer surface collision frequency. In this study, electrostatic forces were neglected but will be included in future models. Additionally, this work forms the foundation for modeling particle augmented mixed-lubrication (PAML), which integrates slurry-nanoparticle dynamics into the complex CMP problem.

Acknowledgment

The authors gratefully acknowledge the support of the Alfred P. Sloan Foundation, Cabot Microelectronics, and the General Motors Fellowship Group for their support of this research. We would also like to thank Professor Shelley Anna for fruitful discussions on particle suspensions.

Nomenclature

a_p = particle radius
D_r = rotary Brownian diffusion coefficient
f_{drag} = drag force on particle from surrounding fluid
f_{gb} = gravity/buoyancy force on particle
f_{hydro} = hydrodynamic force on particle
f_{saff} = Saffman force on particle
g = gravitational acceleration
$h_f(x,t)$ = topography of pad surface
$h_m(x)$ = mean film thickness
h^* = height of particle visualization region in Ng et al. [14]
L = wafer-pad distance in Ng et al. [14]
L_{focus} = horizontal length of each focus area
m_1 = mass of first colliding object
m_2 = mass of second colliding object
m_p = particle mass
MRR = material removal rate
N_P = number of particles in the domain
p = hydrodynamic pressure
Pe = Brownian Peclet number
Re_p = particle Reynolds number
R_p = peak surface roughness
St = impact Stokes number
St_{cr} = critical impact Stokes number
t = simulation time
t_{sim} = total time of particle tracking simulations
T = absolute temperature
Δt = time step
$u(x,y,t)$ or u_f = horizontal velocity of particle-free fluid
u_p = horizontal velocity of particle
u^* = horizontal velocity of particle-free fluid at $y'=h^*$
U = horizontal pad velocity
$v(x,y,t)$ = vertical velocity of particle-free fluid
v_1 = precollision velocity of first colliding object
v_2 = precollision velocity of second colliding object
v_1' = post-collision velocity of first colliding object
v_2' = post-collision velocity of second colliding object
v_p = vertical velocity of particle
V_P = volume of a domain
V_P = volume of a single particle
x = downstream (horizontal distance)
x_p = horizontal location of particle
x_{focus} = horizontal location of the center of the focus area
y = distance from unadjusted wafer surface location toward the pad
y_p = vertical location of particle
y_{wafer} = distance of adjusted wafer surface from original wafer surface
y' = near-wall particle tracking distance for validation simulations
ε = coefficient of restitution
$\varepsilon_{\text{wet}}/\varepsilon_{\text{dry}}$ = ratio between wet and dry coefficient of restitutions
$\dot{\gamma}_m$ = mean shear rate
λ = asperity wavelength
μ = dynamic viscosity of particle-free fluid
ν_s = solid fraction
Ω = angular velocity of inner cylinder in Couette experiments by Shapley et al. [17]
ρ = density of particle-free fluid
ρ_p = density of particle

References

[1] Zhao, Y., and Chang, L., 2002, "A Micro-Contact and Wear Model for Chemical-Mechanical Polishing of Silicon Wafers," Wear, **252**(3-4), pp. 220–226.
[2] Seok, J., Sukam, C. P., Kim, A. T., Tichy, J. A., and Cale, T. S., 2004, "Material Removal Model for Chemical-Mechanical Polishing Considering Wafer Flexibility and Edge Effects," Wear, **257**(5-6), pp. 496–508.
[3] Luo, J. F., and Dornfeld, D. A., 2001, "Material Removal Mechanism in Chemical Mechanical Polishing: Theory and Modeling," IEEE Trans. Semicond. Manuf., **14**(2), pp. 112–133.
[4] Sundararajan, S., Thakurta, D. G., Schwendeman, D. W., Murarka, S. P., and Gill, W. N., 1999, "Two-Dimensional Wafer-Scale Chemical Mechanical Planarization Models Based on Lubrication Theory and Mass Transport," J. Electrochem. Soc., **146**(**2**), pp. 761–766.
[5] Runnels, S. R., and Eyman, L. M., 1994, "Tribology Analysis of Chemical-Mechanical Polishing," J. Electrochem. Soc., **141**(7), pp. 1698–1701.
[6] Cho, C. H., Park, S. S., and Ahn, Y., 2001, "Three-Dimensional Wafer Scale Hydrodynamic Modeling for Chemical Mechanical Polishing," Thin Solid Films, **389**(1-2), pp. 254–260.
[7] Ng, S. H., Borucki, L., Higgs, C. F., Yoon, I., Osorno, A., and Danyluk, S., 2005, "Tilt and Interfacial Fluid Pressure Measurements of a Disk Sliding on a Polymeric Pad," ASME J. Tribol., **127**(1), pp. 198–205.
[8] Tichy, J., Levert, J. A., Shan, L., and Danyluk, S., 1999, "Contact Mechanics and Lubrication Hydrodynamics of Chemical Mechanical Polishing," J. Electrochem. Soc., **146**(4), pp. 1523–1528.
[9] Higgs, III, C. F., Ng, S. H., Borucki, L., Yoon, I., and Danyluk, S., 2005, "A Mixed-Lubrication Approach to Predicting CMP Fluid Pressure Modeling and Experiments," J. Electrochem. Soc., **152**(3), pp. 193–198.
[10] Zhou, C., Shan, L., Hight, J. R., Danyluk, S., Paszkowski, A. J., and Ng, S. H., 2002, "Influence of Colloidal Abrasive Size on Material Removal Rate and Surface Finish in SiO_2 Chemical Mechanical Polishing," Tribol. Trans., **45**(2), pp. 232–238.
[11] Lin, S. C., Kuo, T. C., and Chieng, C. C., 1998, "Particle Trajectories Around a Flying Slider," ASME J. Tribol., **120**(1), pp. 69–74.
[12] Shen, X., and Bogy, D. B., 2003, "Particle Flow and Contamination in Slider Air Bearings for Hard Disk Drives," ASME J. Tribol., **125**(2), pp. 358–363.
[13] Zettner, C. M., and Yoda, M., 2001, "Direct Visualization of Particle Dynamics in Model CMP Geometries," *Proc. of Materials Research Society Symposium*, M. R. Society, Pittsburgh, PA, pp. M6.6.1–M6.6.6.
[14] Terrell, E. J., Garcia, J. I., and Higgs, III, C. F., 2005, "Two-Phase Hydrodynamic Modeling of Particulate Fluids in Sliding Contacts," *Proc. of World Tribology Conference*, American Society of Mechanical Engineers, New York, pp. 511–512.
[15] Lin, J. F., Chen, S. C., Ouyang, Y. L., and Tsai, M. S., 2006, "Analysis of the Tribological Mechanisms Arising in the Chemical Mechanical Polishing of Copper-Film Wafers When Using a Pad With Concentric Grooves," ASME J. Tribol., **128**(3), pp. 445–459.
[16] Ng, S. H., Zettner, C. M., Zhou, C., Yoon, I.-H., Danyluk, S., Sacks, M., and Yoda, M., 2003, "Nanoparticulate and Interfacial Mechanics in Confined Geometries Typical of Chemical-Mechanical Planarization," 2003 ASME International Mechanical Engineering Congress, Nov. 15–21, Washington, DC, ASME, New York, pp. 199–206.
[17] Shapley, N. C., Armstrong, R. C., and Brown, R. A., 2002, "Laser Doppler Velocimetry Measurements of Particle Velocity Fluctuations in a Concentrated Suspension," J. Rheol., **46**(1), pp. 241–272.
[18] Mazaheri, A. R., and Ahmadi, G., 2002, "Modeling the Effect of Bumpy Abrasive Particles on Chemical Mechanical Polishing," J. Electrochem. Soc., **149**(7), pp. 370–375.
[19] Jindal, A., Hegde, S., and Babu, S. V., 2002, "Chemical Mechanical Polishing Using Mixed Abrasive Slurries," Electrochem. Solid-State Lett., **5**(7), pp. 48–50.
[20] Saffman, P. G., 1965, "Lift on Small Sphere in Slow Shear Flow," J. Fluid Mech., **22**(Part 2), pp. 385–400.
[21] Karnis, A., Goldsmith, H. L., and Mason, S. G., 1966, "Flow of Suspensions Through Tubes—5," Can. J. Chem. Eng., **44**(5), pp. 181–193.
[22] Zhang, S., and Bogy, D. B., 1997, "Effects of Lift on the Motion of Particles in the Recessed Regions of a Slider," Phys. Fluids, **9**(5), pp. 1265–1272.
[23] Mewis, J., and Macosko, C. W., 1994, "Suspension Rheology," *Rheology: Principles, Measurements and Applications*, Macosko, C. W., ed., VCH Publishers, New York, pp. 425–474.
[24] Gopal, T., and Talbot, J. B., 2006, "Effects of CMP Slurry Chemistry on the Zeta Potential of Alumina Abrasives," J. Electrochem. Soc., **153**(7), pp. 622–625.
[25] Ramarajan, S., Li, Y., Hariharaputhiran, M., Her, Y. S., and Babu, S. V., 2000, "Effect of pH and ionic Strength on Chemical Mechanical Polishing of Tantalum," Electrochem. Solid-State Lett., **3**(5), p. 232–234.
[26] Davis, R. H., and Serayssol, J.-M., 1986, "Elastohydrodynamic Collision of Two Spheres," J. Fluid Mech., **163**, pp. 479–497.
[27] Gondret, P., Lance, M., and Petit, L., 2002, "Bouncing Motion of Spherical Particles in Fluids," Phys. Fluids, **14**(2), pp. 643–652.
[28] Joseph, G. G., Zenit, R., and Hunt, M. L., 2001, "Particle-Wall Collisions in a Viscous Fluid," J. Fluid Mech., **433**(1), pp. 329–346.
[29] Shan, L., Levert, J., Meade, L., Tichy, J., and Danyluk, S., 2000, "Interfacial Fluid Mechanics and Pressure Prediction in Chemical Mechanical Polishing," ASME J. Tribol., **122**(3), pp. 539–543.